

# Hydrogen bonds induced polymorphism of pyrazoline derivative: Crystal structures, thermal and optical-physical properties

Wenhui Huan, Chao Shen, Qi Feng\*, Guowang Diao

School of Chemistry & Chemical Engineering, Yangzhou University, Yangzhou, 225002, China

## ARTICLE INFO

### Article history:

Received 7 February 2020

Received in revised form

16 June 2020

Accepted 16 June 2020

Available online 29 June 2020

### Keywords:

Polymorphism

Hydrogen bonds

Pyrazoline derivatives

## ABSTRACT

In this study, 1-acetyl-3-(3-hydroxyphenyl)-5-(9-anthracenyl)-2-pyrazoline (AHAP) was synthesized and afforded two types of polymorphs. Single crystal X-ray analyses revealed that AHAP molecules connect with each other in a head-to-tail fashion through O-H...O hydrogen bonds between the carbonyl and hydroxyl groups. However, through the above intermolecular interactions and stacking mode, the one-dimensional chain motifs are formed in the  $\alpha$  polymorph and cyclic tetramers are formed in the  $\beta$  polymorph, which constitute their crystal structures as units. Compared with solvent-free  $\alpha$  polymorph, the unit cell of the  $\beta$  polymorph includes a small region of disordered solvent molecules. CrystalExplorer program, Differential scanning calorimetry (DSC) and thermogravimetric thermal analysis (TGA) experiments revealed that the voids should be inside the tetramers and each void contains one disordered solvent molecule.  $^1\text{H}$  NMR spectra conformed the type of the disordered solvent molecule is consistent with the crystalline liquid phase. The optical-physical properties of the two polymorphs were also investigated. They emit similar fluorescence, which is assigned to monomer emission of anthracene, due to the monomer arrangement of anthracene fluorophores in the two polymorphs.

© 2020 Elsevier B.V. All rights reserved.

## 1. Introduction

Organic luminescent materials have recently attracted considerable attention due to their excellent optical-physical properties [1–4]. However, many fluorophores that exhibit bright fluorescence in solution usually suffer fluorescence quenching in the solid state [5,6], because the molecular aggregation usually leads to formation of the species, such as excimers or exciplexes [7,8], which are detrimental to luminescence. Therefore, the enhancement of their optical-physical properties has been a subject of great interest from both academia and industry [9,10]. Current research on the fluorescent materials indicated the solid optical-physical properties are usually closely related to arrangement of the fluorophores [11], thus the regulation of fluorophores' stacking mode without changing their chemical structure is one of convenient methods for tuning their solid optical-physical properties, which could avoid complex synthesis process [12].

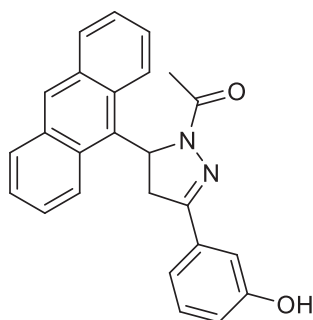
Polymorphism is a common phenomenon of the organic compounds, which is known as the ability to yield different crystal

forms of a given compound [13–15]. The different polymorphs usually have various physicochemical properties, such as melting point, color and optical-physical properties [16,17]. Previously, our group have investigated the polymorphism of several 1-acetylpyrazoline derivatives [18–20]. In these study, we found that the hydrogen bonds formed by carbonyl group always affect molecular arrangement. On the one hand, the different weak intermolecular hydrogen bonds between carbonyl groups and hydrogen atoms affect self-arrangement of these pyrazoline derivatives, which lead to the formation of different polymorphs. On the other hand, carbonyl groups could form strong hydrogen bonds with other solvent molecules containing active hydrogen atoms, such as various carboxylic acids, and yield corresponding solvates (pseudopolymorphs). Through above strategy, arrangement of the fluorophores was regulated and their solid optical properties was also improved.

Due to the obvious effect on molecular arrangement by hydrogen bonds, in this study we synthesized a new pyrazoline derivative: 1-acetyl-3-(3-hydroxyphenyl)-5-(9-anthracenyl)-2-pyrazoline (AHAP), which contains a pair of hydrogen bond donor and acceptor Scheme 1. On the one hand, we wanted to investigate the self-stacking mode of pyrazoline molecules induced by strong O-H...O hydrogen bonds between the carbonyl and hydroxyl

\* Corresponding author.

E-mail address: 006450@yzu.edu.cn (Q. Feng).



**Scheme 1.** Chemical structures of AHAP molecule.

groups. On the other hand, we expected to discover whether other interactions could affect the molecular arrangement by competing with the hydrogen bonds and yield the different polymorphs. To our surprise, the O-H...O hydrogen bonds not only mainly affect arrangements of AHAP molecules, but also results in formation of two polymorphs. Through the O-H...O hydrogen bonds, AHAP molecules connect with each other in a head-to-tail fashion, and form one-dimensional chain motifs in the  $\alpha$  polymorph and cyclic tetramers in the  $\beta$  polymorph, which are identified as the units that form their crystal structures, respectively. To the best of our knowledge, the analogous polymorphism was rarely reported [21]. The crystal structures of the two polymorphs was described and discussed in the text. In addition, the polymorphic transition in this study could be only discovered at comparatively higher temperature (>250 °C) in the thermal analysis experiments, and no phase transition could be found under other conditions, such as grinding. Thus the stability of the two polymorph was investigated by theoretical calculation method. Furthermore, the optical-physical properties of two polymorphs were also investigated.

## 2. Experiment

### 2.1. Material synthesis and characterization

The AHAP molecule was synthesized by a previous reported method [22]. A mixture of 3-hydroxyacetophenone (1.6 g), 9-anthracenecarboxaldehyde (2.3 g), and 3 M of aqueous sodium hydroxide (6 mL) in ethanol (20 mL) was stirred at 50 °C for 16 h. The resulting solid was filtered to afford 3-(anthracen-9-yl)-1-(3-hydroxyphenyl)prop-2-en-1-one, which was used directly without purification. The chalcone (1 g) and 80% hydrazine hydrate (3.5 g) were dissolved in glacial acetic acid (20 mL). The mixture was stirred under reflux condition for 5 h, and the resulting solution was cooled and poured slowly into a beaker containing ice water. The crude product was collected by filtration and recrystallized from ethyl acetate to give pure AHAP as yellow powder: 0.78 g, yield: 67.2%, m.p.: 286–288 °C,  $^1\text{H}$  NMR (Fig. S1 in the Supporting Information):  $\delta$  (ppm) 2.19 (s, 3H), 3.36–3.46 (q, 1H), 4.05–4.21 (q, 1H), 6.85–6.92 (t, 2H), 7.22–7.34 (m, 3H), 7.36–7.47 (m, 2H), 7.51–7.62 (m, 2H), 7.68–7.73 (d, 2H), 8.08–8.13 (d, 1H), 8.55–8.63 (d, 2H), 9.70 (s, 1H).

### 2.2. Crystallization

The two polymorphs were obtained in different solvents by solvent evaporation method (Table 1). 1 g AHAP was dissolved in 20 mL solvents in glass vials. Slow evaporation of the solvents at room temperature for 4–5 days yielded the needle ( $\alpha$  polymorph) and prism ( $\beta$  polymorph) crystals.

**Table 1**  
Polymorph screening of AHAP.

solvent	product
ethyl acetate	$\alpha$ polymorph
acetonitrile	$\alpha$ polymorph
chloroform	$\alpha$ polymorph
acetone	$\beta$ polymorph
ethanol	$\beta$ polymorph

### 2.3. Measurement

$^1\text{H}$  NMR spectra were recorded at room temperature on a Bruker Avance 600 MHz NMR spectrometer using DMSO as a solvent and TMS as an internal standard. Powder X-ray diffraction (PXRD) patterns for the two polymorphs were recorded using an 18 kW advance X-ray diffractometer with Cu K $\alpha$  radiation ( $\lambda = 1.54056 \text{ \AA}$ ). Single-crystal X-ray diffraction experiments were carried out using a Bruker D8 QUEST diffractometer with a graphite-monochromatized Mo K $\alpha$  radiation ( $\lambda = 0.71073 \text{ \AA}$ ). Data collection for two types of polymorphs were done at ambient temperature. Crystal structures were solved by the direct methods SHELXS and refined anisotropically by a full-matrix least-squares SHELXL [23]. All non-hydrogen atoms were refined anisotropically and hydrogen atoms were inserted at their calculated positions and fixed at their positions. The structural data for the two polymorphs have been deposited as CIFs at the Cambridge Crystallographic Data Base (CCDC No. 1855433 and 1965213) and are also available as Supporting Information (SI).

For the  $\beta$  polymorph, electron density associated with additional disordered solvent molecules was removed by means of the SQUEEZE procedure of PLATON program [24,25]. Take the products crystallized from ethanol as an example, SQUEEZE estimated the solvent-accessible volume is  $728 \text{ \AA}^3$  and the number of electrons is 92 (23 electrons per  $182 \text{ \AA}^3$ ), which is in good agreement to be four ethanol molecules in the unit cell ( $Z = 16$ ;  $\text{CH}_3\text{CH}_2\text{OH} = 26e^-$ ;  $92e^- \approx 4 \text{ CH}_3\text{CH}_2\text{OH}$ ), namely the molar ratio of AHAP and ethanol molecules is 1:4. The disordered solvent molecules were not taken into account during refinement.

Differential scanning calorimetry (DSC) and thermogravimetric thermal analysis (TGA) patterns were recorded with a Mettler-Toledo Thermogravimetric Analyzer with the temperature scanned from 50 to 500 °C at a heating rate of 10 °C/min. For each measurement, about 5–6 mg of dried sample was placed inside an aluminum pan with a lid. Hot stage microscopy was performed on a LEICA DM750P microscope using a Mettler-Toledo FP82HT hot stage. UV–vis absorption spectra were recorded on a Shimadzu UV-3600 spectrometer. Fluorescence spectra were obtained on a Horiba FluoroMax 4 spectrofluorometer.

### 2.4. Theoretical calculation method

The geometry optimization of crystals was performed starting from the X-ray structures. Cambridge Sequential Total Energy Package (CASTEP) module based on the Planewaves Pseudopotential method of density functional theory (DFT) was used to optimize the two polymorphs, all lattice constants and atomic coordinates were relaxed until the force on each atom converges within 0.01 eV/Å and the local energy minimum of these structures are calculated. Generalized Gradient Approximation (GGA) and Perdew-Burke-Ernzerhof (PBE) exchange-correlation functional were used. To ensure the correctness of the calculation, the cut-off energy was selected as 400.0 eV and the k-point grid was set as  $3 \times 3 \times 2$ . All the calculations were performed by Material Studio 6.0 program [26].

### 3. Result and discussion

#### 3.1. $^1\text{H}$ NMR spectra

For  $^1\text{H}$  NMR spectrum of AHAP molecule (Fig. S1), the singlet signals observed at  $\delta_{\text{H}}$  2.19 was assigned to methyl group, while singlet signals at  $\delta_{\text{H}}$  3.32 and 4.09 were ascribed to the two protons in methylene group. The signals at  $\delta_{\text{H}}$  6.89 was assigned to methine group, which overlapped with the aromatic protons. Multiple signals (13H) from 6.9 to 8.7 ppm were attributed to the aromatic protons in benzyl and anthryl, respectively. The singlet signals at  $\delta_{\text{H}}$  9.70 was assigned to phenolic hydroxyl protons. Moreover, in  $^1\text{H}$  NMR spectra of the  $\beta$  polymorphs crystallized separately from ethanol and acetone solvents, the extra peaks at  $\delta_{\text{H}}$  1.24 and 2.06 could be clearly observed, which correspond to  $\text{CH}_3^-$  (ethanol) and  $\text{CH}_3^-$  (acetone) groups, suggesting the disordered solvent molecules enclosed in  $\beta$  polymorph are consistent with the crystalline liquid phase (Figs. S2 and S3).

#### 3.2. Crystal structures

Single crystal X-ray diffraction analyses were performed for the two polymorphs to determine their crystal structures. Thermal ellipsoids of AHAP molecules in the  $\alpha$  and  $\beta$  polymorphs were displayed in Fig. 1. All the AHAP molecules exhibit twisted structures, the dihedral angles between the anthracene and benzene rings are  $75.96^\circ$  ( $\alpha$  polymorph) and  $80.34^\circ$  ( $\beta$  polymorph), respectively. In addition, no strong  $\pi$ - $\pi$  interaction between the anthracene fluorophores was found in both of two polymorphs, the closest centroid distance is 4.010 and 6.279 Å, respectively. The crystallographic data was presented in Table 2.

The  $\alpha$  polymorph has a monoclinic system and space group  $P2_1/c$ . The unit cell parameters are  $a = 10.369(3)$  Å,  $b = 12.426(4)$  Å,  $c = 15.9836(14)$  Å,  $\beta = 108.82^\circ$  and  $Z = 4$ . The heterochiral AHAP molecules associate alternately through O-H $\cdots$ O hydrogen bonds between the carbonyl and hydroxyl groups to form a racemic chain motif. The hydrogen bond geometry has  $R_{\text{H}\cdots\text{O}} = 1.933$  Å,  $R_{\text{O}\cdots\text{O}} = 2.746$  Å, and  $\angle\text{O-H}\cdots\text{O} = 171.45^\circ$ . These chains connect with each other through C-H $\cdots$  $\pi$  interactions along the  $b$  axis, which are stacked in a parallel fashion to form its three-dimensional structure (Fig. 2).

The  $\beta$  polymorph crystallizes in a tetragonal system with the space group  $I4_1/a$ . The unit cell parameters are  $a = 22.890(2)$  Å,  $b = 22.890(2)$  Å,  $c = 15.9836(14)$  Å, and  $Z = 16$ . The main structural units are cyclic tetramers (Fig. 3a), which are composed of two pairs of  $R/S$ -AHAP molecules and linked by four O-H $\cdots$ O hydrogen bonds between the carbonyl and hydroxyl groups. The hydrogen bond geometry has  $R_{\text{H}\cdots\text{O}} = 1.933$  Å,  $R_{\text{O}\cdots\text{O}} = 2.746$  Å, and  $\angle\text{O-H}\cdots\text{O} = 171.45^\circ$ . As shown in Fig. 3b, it could be clearly observed that the three-dimensional structure of  $\beta$  polymorph is composed of the tetramers arranged in a parallel fashion. The

**Table 2**  
Numerical details of the solutions and refinements of the two polymorphs.

Crystals	$\alpha$	$\beta$
Formula	$\text{C}_{25}\text{H}_{20}\text{N}_2\text{O}_2$	$\text{C}_{25}\text{H}_{20}\text{N}_2\text{O}_2$
Morphology	needle	prism
Crystal system	monoclinic	tetragonal
Space group	$P2_1$	$I4_1/a$
$a/\text{Å}$	10.369(3)	22.890(2)
$b/\text{Å}$	12.426(4)	22.890(2)
$c/\text{Å}$	16.068(5)	15.9836(14)
$\alpha/\text{deg}$	90	90
$\beta/\text{deg}$	108.82	90
$\gamma/\text{deg}$	90	90
$V/\text{Å}^3$	1959.6(10)	8374.6(17)
$Z$	4	16
$\rho$ (calcd)/ $\text{Mg m}^{-3}$	1.290	1.207
$\theta$ Range for data collection/ $^\circ$	2.64–25.97	2.36–22.92
$F(000)$	800	3200
$R_1, wR_2$ ( $I > 2\sigma(I)$ )	0.0589, 0.1384	0.0579, 0.1476
$R_1, wR_2$ (all data)	0.1185, 0.1628	0.1288, 0.1679
Goodness-of-fit, $S$	1.029, 1.029	1.026, 1.026
CCDC	1855433	1965213

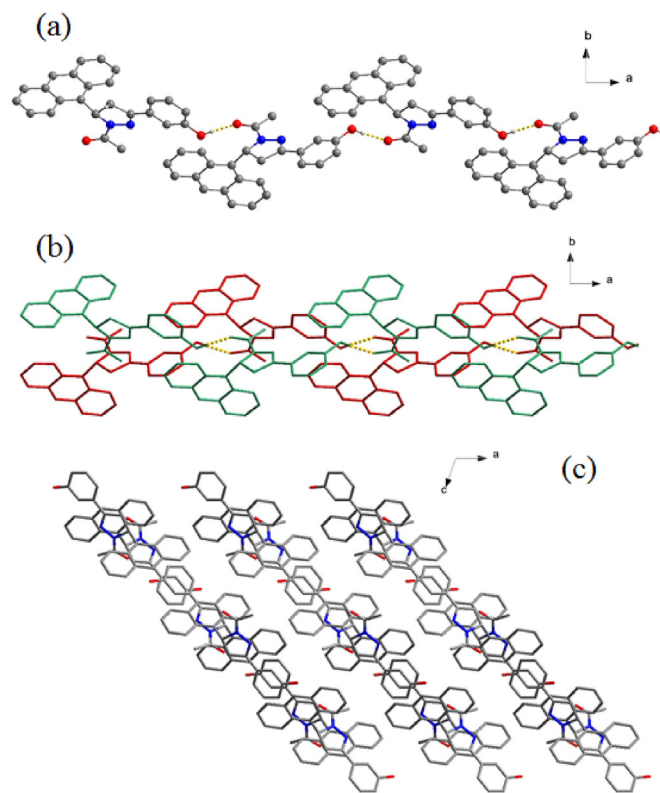


**Fig. 2.** Crystal structure of the  $\alpha$  polymorph: (a) 1D racemic chain motif via hydrogen bonds. (b) Arrangement of the racemic chains. (c) 3D packing diagram of the  $\alpha$  polymorph (projected in the  $ac$  plane).

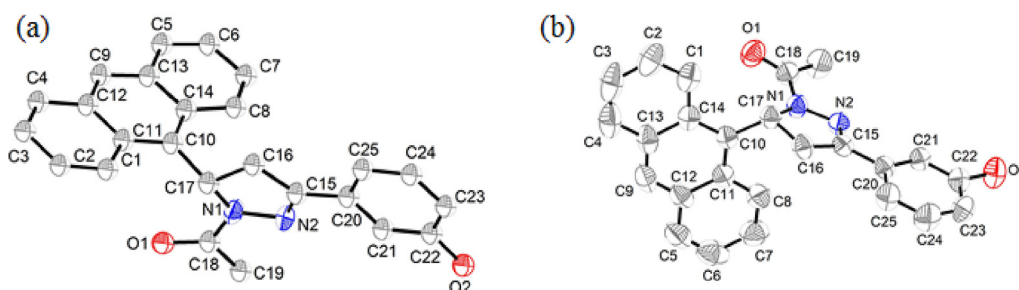


**Fig. 1.** Thermal ellipsoids plot of the  $\alpha$  polymorph (a) and  $\beta$  polymorph (b).

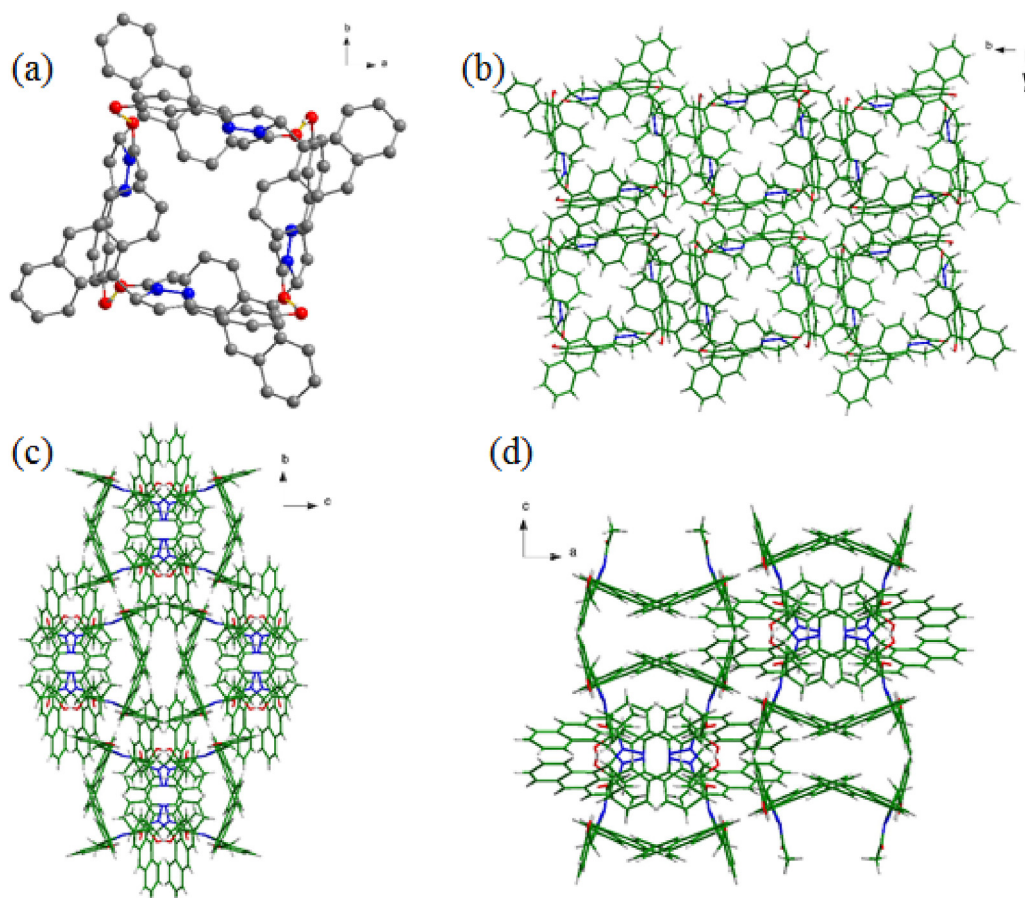


**Fig. 3.** Crystal structure of the  $\beta$  polymorph: (a) The cyclic tetramer via hydrogen bonds. (b–d) 3D packing diagram of the  $\beta$  polymorph (projected in the  $ab$ ,  $bc$  and  $ac$  plane).

projection of the crystal lattice on to the  $bc$  and  $ac$  plane was presented in Fig. 3c and d, respectively.

The analyses of voids in the  $\beta$  polymorph was performed with CrystalExplorer program, this program was also used to investigate Hirshfeld surfaces [27]. According to the depiction by CrystalExplorer, it was not possible to observe significant channels in the  $\beta$  polymorph (Fig. 4), although it appears from Fig. 3 that there seem to be some small channels. Thus we speculated the voids should be inside the tetramers and the disorder solvent molecules were also considered to be included in these isolated voids.

Hirshfeld surface was performed to give insights regarding the important intermolecular interactions in the two polymorphs. As shown in Fig. 5a and b, it could be observed that all the AHAP molecules in the two polymorphs exhibit two red spots on the phenolic hydroxyl and carbonyl groups, which correspond to O-

H $\cdots$ O hydrogen bonds for constructing the racemic chain motif ( $\alpha$  polymorph) and cyclic tetramer ( $\beta$  polymorph). This result further conformed that the O-H $\cdots$ O hydrogen bonds mainly affect molecular stacking mode in the two polymorphs. Moreover, it is noteworthy that the opposite directions of the hydrogen atoms on the phenolic hydroxyl groups in the two polymorphs, which leads to the different arrangements of AHAP molecules and could be considered as one of the reasons for construction of the two different crystal forms.

Table 3 summarized the contacts contributing to the Hirshfeld surface represented in normal mode. It was found that weak H $\cdots$ H contacts displays the major contribution in the two polymorphs, with 53.1% and 50.9% of total surface area, respectively. The C $\cdots$ H contacts with second major contribution comprise 24.4% and 33.3% of total surface area. Apart from that, O $\cdots$ H contacts in the two

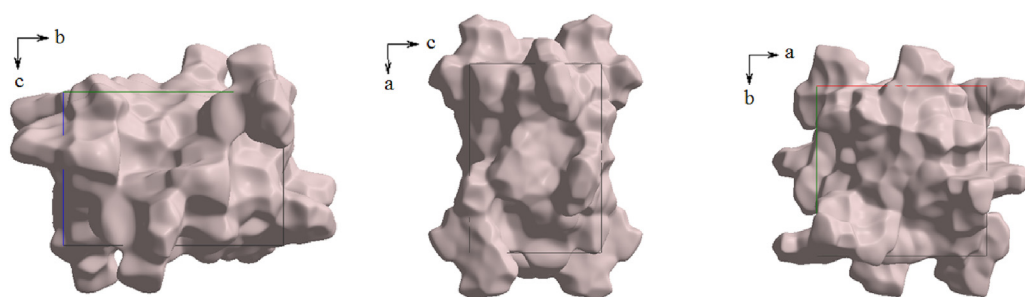


**Fig. 4.** The analysis of voids for the  $\beta$  polymorph.

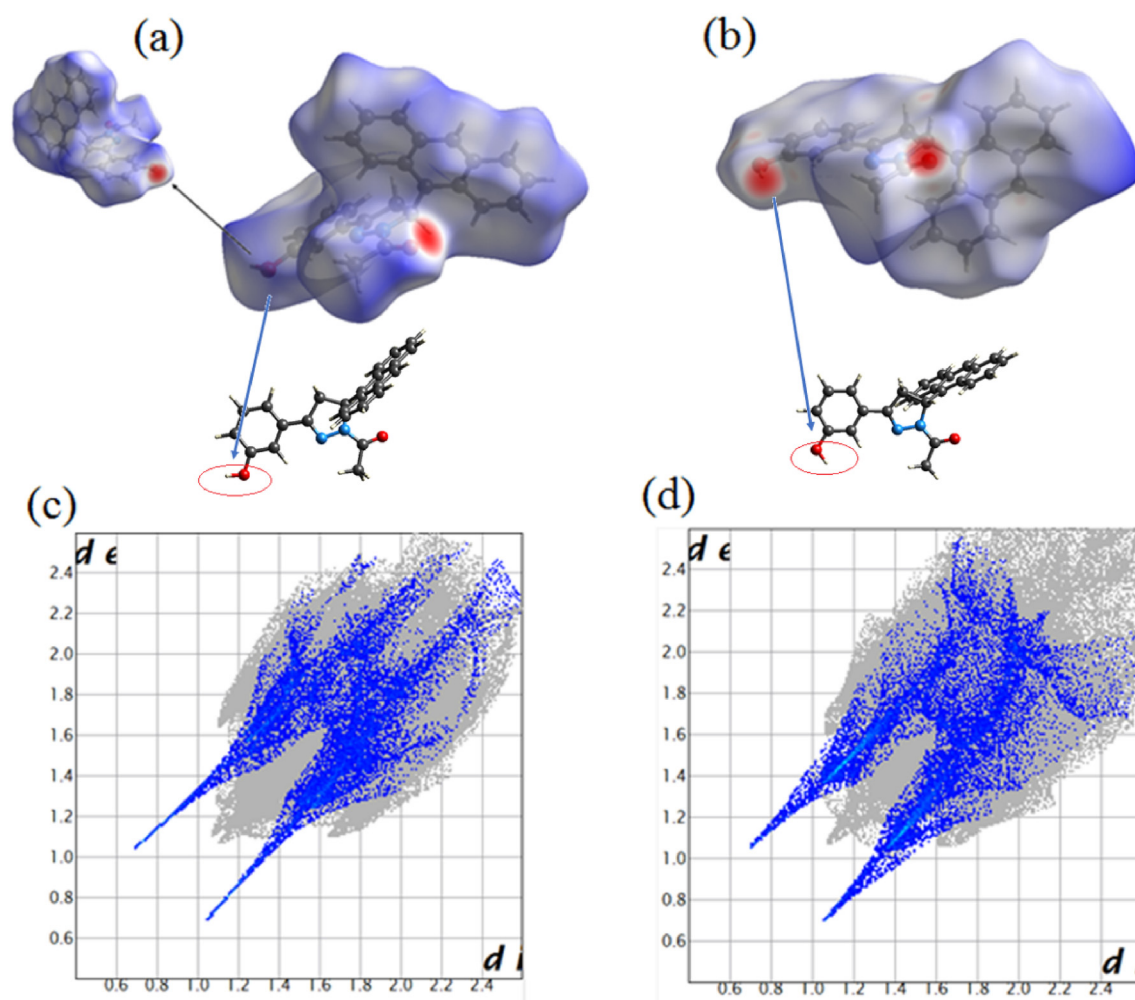


**Fig. 5.** Hirshfeld surface mapped with  $d_{\text{norm}}$  for the AHAP molecules and two-dimensional fingerprint plots for  $\text{O}\cdots\text{H}/\text{H}\cdots\text{O}$  contacts in the  $\alpha$  polymorph (a, c) and  $\beta$  polymorph (b, d).

**Table 3**

Contributions of the intermolecular contacts.

AHAP molecule	H...H %	C...H %	O...H %	N...H %	C...N %	C...C %	C...O %
$\alpha$ polymorph	53.1	24.4	11.7	0.9	1.6	6.2	2.0
$\beta$ polymorph	50.9	33.3	12.1	0.4	1.4	1.2	0.6

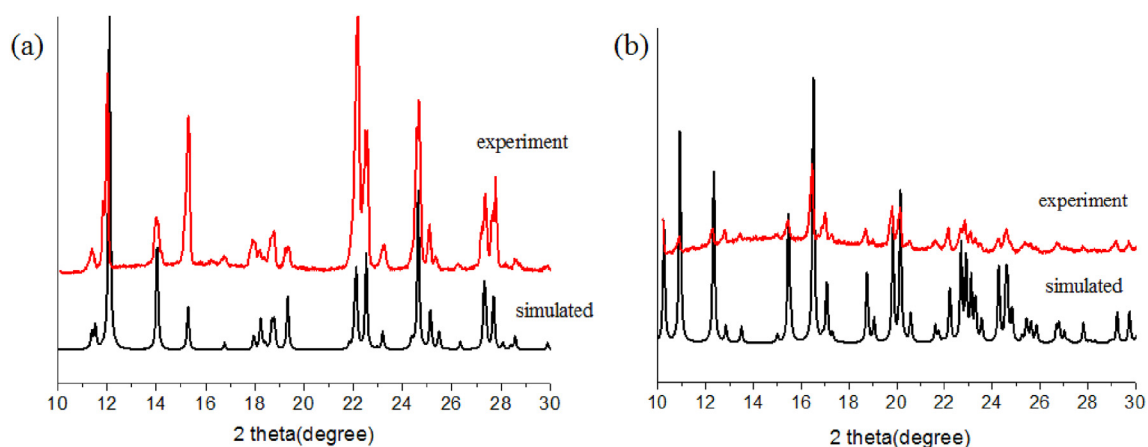


**Fig. 6.** The experiment and simulated PXRD patterns of  $\alpha$  polymorph (a) and  $\beta$  polymorph (b).

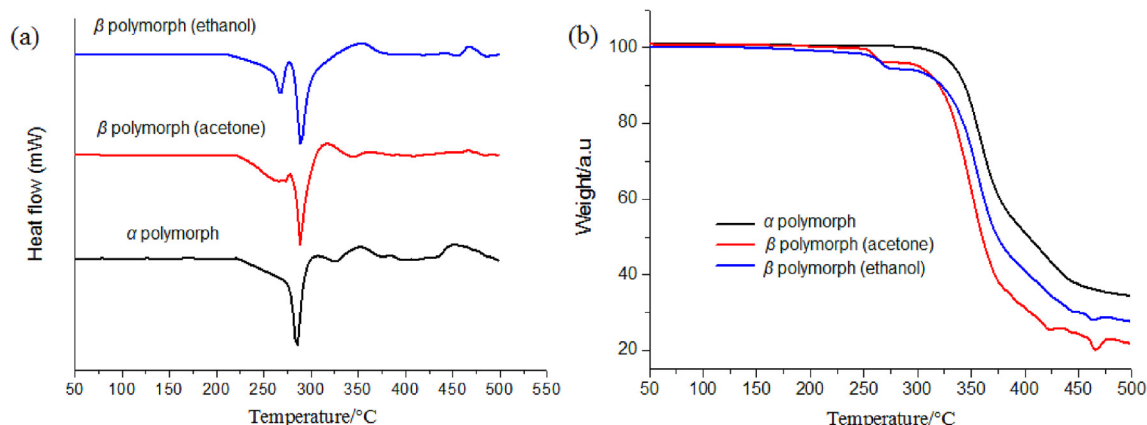


Fig. 7. (a) DSC and (b) TGA profiles of the  $\alpha$  polymorph and the  $\beta$  polymorph crystallized from ethanol and acetone solvents.

Table 4

The energy (eV) of the two polymorphs calculated by GGA PBE method.

Crystals	Energy
$\alpha$ polymorph	-44869.6204
$\beta$ polymorph	-44867.5635

polymorphs also exhibits important contribution for the supra-molecular architectures as 11.7 and 12.1% of total surface area and appears as two wings in the left (H $\cdots$ O) and right (O $\cdots$ H) areas of the related plots (Fig. 5c and d).

### 3.3. Powder X-ray diffraction (PXRD) patterns

The powder samples of the two polymorphs were characterized by powder X-ray diffraction. Prior to recording PXRD patterns, powders were gently pressed onto a glass slide to give a flat surface. The data were collected over the  $2\theta$  range 3–30° at ambient temperature. As shown in Fig. 6, the experimental PXRD patterns of the two polymorphs matched well with their simulated PXRD patterns, which indicate that the samples have high purity. In addition, PXRD patterns of the  $\beta$  polymorphs crystallized from ethanol and acetone solvents are identical, indicating no structural changes in the crystallinity of the samples contained different disordered solvent molecules (Fig. S4).

### 3.4. Thermal properties

The thermal properties of the two polymorphs were investigated by DSC and TGA experiments. The  $\alpha$  polymorph exhibits only one endothermic peak at 289 °C in its DSC pattern, and no obvious weight loss could be observed until 289 °C in its TGA pattern, suggesting that it belongs to solvent-free crystal and begins to decompose at 289 °C (Fig. 7).

The  $\beta$  polymorph crystallized from ethanol solution shows two endothermic peaks at 267 and 289 °C in its DSC pattern, and one-step decomposition can be observed weight loss of 2.77% around 267 °C in the TGA pattern. The step is in good agreement with calculations for the release of disordered ethanol molecules [ $\Delta m_{\text{calc}}(\text{CH}_3\text{CH}_2\text{OH}) = 2.93\%$ , the molar ratio of AHAP and ethanol is 4:1]. The analogous endothermic event was found in the DSC and TGA patterns of  $\beta$  polymorph crystallized from acetone, one-step weight loss of 3.47% could be also observed around 254 °C, corresponding to the release of the acetone molecules [ $\Delta m_{\text{calc}}(\text{CH}_3\text{COCH}_3) = 3.67\%$ , the molar ratio of AHAP and acetone is 4:1]. The removal of the disordered solvent molecules was found to be at comparatively higher temperatures (>250 °C), suggesting the solvent molecules should be enclosed in the voids, namely these molecules could not be removed until the decomposition of AHAP tetramers.

Previous research has suggested that thermal analysis can be used as a tool for determining polymorph types [28,29]. The DSC and TGA patterns of  $\beta$  polymorph after solvent removal are exactly

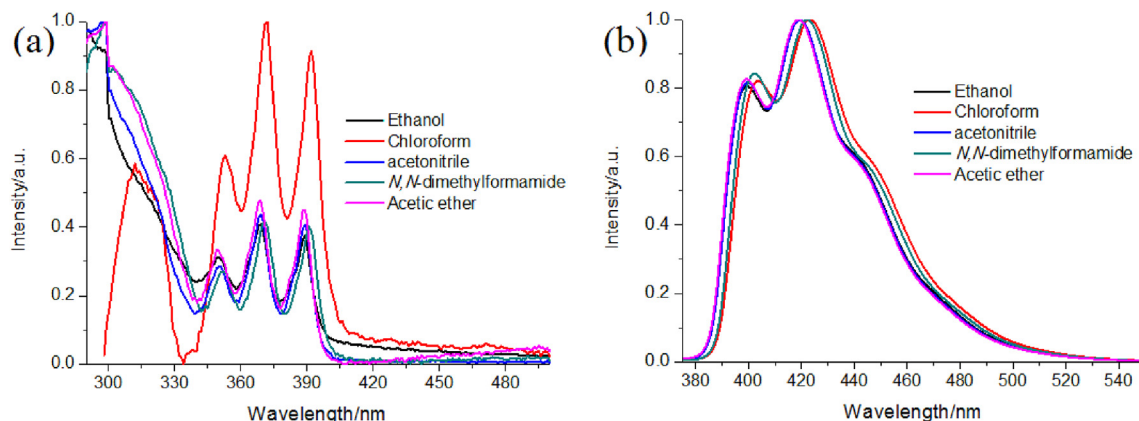


Fig. 8. UV-Vis (a) and fluorescence (b) spectra of the AHAP molecule in various solvents.

**Table 5**  
Optical-physical properties data.

solvents/crystals	$\lambda_{ab}$ (nm) <sup>a</sup>	$\lambda_{em}$ (nm) <sup>b</sup>
ethanol	368	419
chloroform	371	423
acetonitrile	369	419
<i>N,N</i> -dimethylformamide	370	421
acetic ether	368	419
$\alpha$ polymorph	251	433
$\beta$ polymorph	252	428

<sup>a</sup> Maximum wavelengths of absorption spectra.<sup>b</sup> Fluorescent quantum yields excited at 365 nm.

the same as that of  $\alpha$  polymorph, thus these products were characterized by PXRD measurement. As expected, the PXRD results clearly demonstrated that the products could be identified as the  $\alpha$  polymorph, due to their identical patterns (Fig. S5). In fact, the phase transition experiments were also tried to achieve through using grinding methods. However, the transition could be only observed during the DSC experiments. In order to approach the reason, the theoretical calculation was performed to give insights regarding the stability of the two polymorphs. Fixed the unit cell parameters, the AHAP molecules were relaxed to obtain the energy of each unit cell. The result (Table 4) exhibited the  $\alpha$  polymorph is more stable, and the  $\beta$  polymorph needs to overcome 47.4321 kcal/mol (2.0569 eV) for transforming into the  $\alpha$  polymorph. Such much energy difference may be the reason that the phase transition only occurs under high temperature condition in this study.

### 3.5. Optical-physical properties

The absorption and fluorescence spectra of AHAP in various solvents with different polarities were shown in Fig. 8, the optical-physical data was summarized in Table 5. The absorption spectra of AHAP have little change with an increase in the solvent polarity and are similar with that of anthracene, which are structured with band maxima slightly red-shifted (Fig. 8a). The fluorescence spectra in various solvents were presented in Fig. 8b. Be similar with the absorption spectra, no obvious difference could be observed in the fluorescence spectra, which exhibits vibrational peaks at about 400 and 420 nm and weak shoulders around 445 nm, corresponding to anthracene chromophore emission. The results of optical-physical investigation in solution system showed that the fluorescence

arises from anthracene fluorophores and no strong intramolecular charge transfer occurs in the photo-physical process.

The solid state optical-physical properties of  $\alpha$  and  $\beta$  polymorphs were also investigated. As shown in Fig. 9a,  $\alpha$  and  $\beta$  polymorphs have similar absorption spectra, which exhibit broad absorption bands around 250 and 310 nm, respectively. Compared with that measured in solvents, the intensity of weak characteristic absorption bands of anthracene in 350–400 nm range become greatly weak. The two polymorphs also exhibit similar fluorescence in the solid-state (Fig. 9b). Be different from their absorption spectra, the emission band is similar with that in solvents, which should be assigned to monomer emission of anthracene. As mentioned above, the fluorescence of AHAP arises from anthracene fluorophores, thus the optical properties are closely related to anthracene's arrangement. In the crystal structures of two polymorphs, no strong interaction, such as  $\pi$ - $\pi$  interaction, was discovered among the anthracene fluorophores, which may be the reason that two polymorphs still exhibit anthracene monomer emission and their similar fluorescence.

## 4. Conclusions

In summary, we discovered an interesting polymorphism in 1-acetyl-3-(3-hydroxyphenyl)-5-(9-anthracenyl)-2-pyrazoline (AHAP). The O-H...O hydrogen bonds mainly affect molecular arrangement and results in formation of two different polymorphs. Although AHAP molecules in both two polymorphs connect with each other in a head-to-tail fashion, they form one-dimensional chain motifs in the  $\alpha$  polymorph and cyclic tetramers in the  $\beta$  polymorph, which constitute their crystal structure as units. This unique phenomenon was rarely reported previously. <sup>1</sup>H NMR, CrystalExplorer program, DSC and TGA experiments were used to investigate the two polymorphs. The results revealed that the  $\alpha$  polymorph belongs to the solvent-free crystal and the  $\beta$  polymorph contains the voids and disordered solvent molecules. The voids should be inside the tetramers and each void contains one solvents molecule. Furthermore, the phase transition between the two polymorphs only occurs under the high temperature, because the disordered solvent molecules could not be removed except decomposition of tetramers. The optical-physical properties of two polymorphs were also investigated. Due to the monomer arrangement of anthracene fluorophores, they emit similar fluorescence spectra assigned to anthracene's monomer emission.

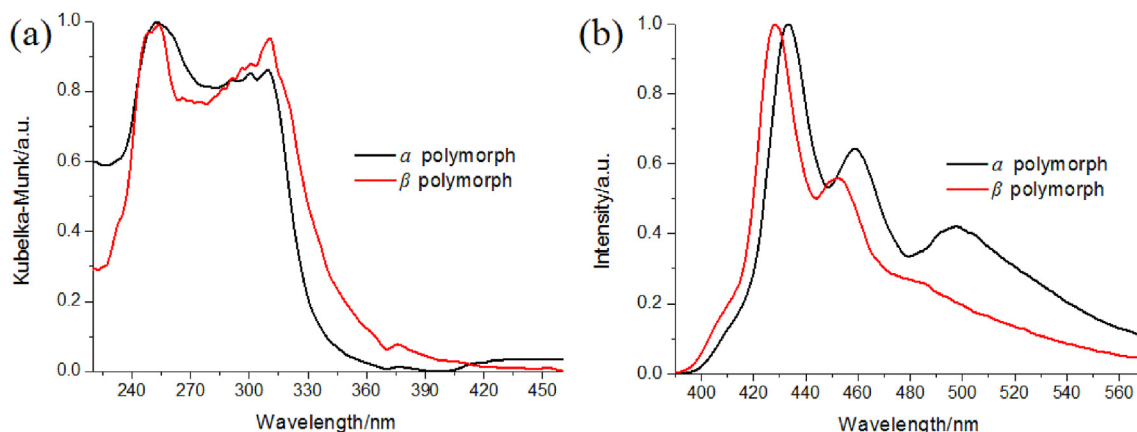


Fig. 9. Absorption (a) and fluorescence (b) spectra of  $\alpha$  and  $\beta$  polymorphs.

## CRediT authorship contribution statement

**Wenhui Huan:** Methodology, Data curation. **Chao Shen:** Investigation, Software. **Qi Feng:** Funding acquisition, Investigation, Writing - original draft, Writing - review & editing. **Guowang Diao:** Funding acquisition.

## Declaration of competing interest

There are no conflicts to declare.

## Acknowledgements

This work is partly supported by the National Natural Science Foundation of China (Grant No. 21773203), Certificate of China Postdoctoral Science Foundation Grant (No. 2018M632387), the Natural Science Foundation of the Jiangsu Higher Education Institutions of China (No. 18KJB150035), and Innovation and Cultivation Fund of Yangzhou University (No. 2017CXJ012), Jiangsu Provincial Department of Education.

## Appendix A. Supplementary data

Supplementary data to this article can be found online at <https://doi.org/10.1016/j.molstruc.2020.128725>.

## References

- [1] A. Genco, A. Ridolfo, S. Savasta, S. Patane, G. Gigli, M. Mazzeo, Bright polariton coumarin-based OLEDs operating in the ultrastrong coupling regime, *Adv. Opt. Mater.* 6 (2018) 1800364.
- [2] L.Q. Yan, R.J. Li, W. Shen, Z.J. Qi, Multiple-color AIE coumarin-based Schiff bases and potential application in yellow OLEDs, *J. Lumin.* 194 (2018) 151–155.
- [3] T.Z. Yu, Z.Y. Zhu, Y.J. Bao, Y.L. Zhao, X.X. Liu, H. Zhang, Investigation of novel carbazole-functionalized coumarin derivatives as organic luminescent materials, *Dyes Pigments* 147 (2017) 260–269.
- [4] D.F. Dang, X.C. Wang, D.Q. Wang, Z.W. Yang, D.X. Hao, Y.Z. Xu, S. L. Zhang, L.J. Meng, Fluorescent organic nanoparticles constructed by a facile “self-isolation enhanced emission” strategy for cell imaging, *ACS Appl. Nano Mater.* 1 (2018) 2324–2331.
- [5] B.S. Fu, J.G. Huang, D.S. Bai, Y.L. Xie, Y. Wang, S.R. Wang, X. Zhou, Label-free detection of pH based on the i-motif using an aggregation-caused quenching strategy, *Chem. Commun.* 51 (2015) 16960–16963.
- [6] Y.J. Huang, J. Xing, Q.Y. Gong, L.C. Chen, G.F. Liu, C.J. Yao, Z.R. Wang, H.L. Zhang, Z. Chen, Q.C. Zhang, Reducing aggregation caused quenching effect through co-assembly of PAH chromophores and molecular barriers, *Nat. Commun.* 10 (2019) 1–9.
- [7] F.M. Winnik, Photophysics of preassociated pyrenes in aqueous polymer solutions and in other organized media, *Chem. Rev.* 93 (1993) 587–614.
- [8] T.C. Chou, C.L. Hwa, J.J. Lin, K.C. Liao, J.C. Tseng, Bicyclo [2.2.2] octene-based “crab-like” molecules: synthesis, complexation, luminescence properties, and solid-state structures, *J. Org. Chem.* 70 (2005) 9717–9726.
- [9] H. Jin, H. Li, Z. Zhu, J. Huang, Y. Xiao, Y. Yan, Hydration-facilitated fine-tuning of the AIE amphiphile color and application as erasable materials with hot/cold dual writing modes, *Angew. Chem. Int. Ed. Engl.* 59 (25) (2020) 10081–10086.
- [10] L. Viglianti, N. Xie, H.H.Y. Sung, A.A. Voityuk, N.L.C. Leung, Y. Tu, C. Baldoli, I.D. Williams, R.T.K. Kwok, J.W.Y. Lam, E. Licandro, L. Blancafort, B.Z. Tang, Unusual through-space interactions between oxygen atoms that mediate inverse morphochromism of an AIE luminogen, *Angew. Chem. Int. Ed. Engl.* 59 (22) (2020) 8552–8559.
- [11] T.L. Zhou, T. Jia, S.S. Zhao, J.H. Guo, H.Y. Zhang, Y. Wang, Acid-stimuli-luminescence and carbonyl-proton interaction dependent emission properties of 2, 6-biphenyl-4-pyrone crystals, *Cryst. Growth Des.* 12 (2012) 179–184.
- [12] W.G. Xi, Y.M. Gong, B. Mei, X.Z. Zhang, Y.B. Zhang, B.Y. Chen, J.Y. Wu, Y.P. Tian, H.P. Zhou, Schiff base derivatives based on diaminomaleonitrile: colorimetric and fluorescent recognition of Cu (II), cell imaging application, polymorph-dependent fluorescence and aggregation-enhanced emission, *Sensor. Actuator. B Chem.* 205 (2014) 158–167.
- [13] H.R. Bloomfield, J.S. Ritch, A new polymorph of phenylselenium trichloride, *Acta Crystallogr.* 75 (2019) 1471–1474.
- [14] V.M. Zemtsova, A.Y. Fedorov, E.A. Fedorova, C. Boa, S.G. Arkhipov, D.A. Rychkov, V.S. Minkov, C.R. Pulham, E.V. Boldyreva, A novel crystal form of metacetamol: the first example of a hydrated form, *Acta Crystallogr.* 75 (2019).
- [15] N. Bolotina, O. Yakubovich, L. Shvanskaya, O. Dimitrova, A. Volkov, A. Vasiliev, A commensurately modulated crystal structure and the physical properties of a novel polymorph of the caesium manganese phosphate CsMnPO<sub>4</sub>, *Acta Crystallogr.* 75 (2019) 822–829.
- [16] M. Singh, R. Bhowal, R. Vishwakarma, D. Chopra, Assessing the impact on aqueous solubility of berberine chloride via co-crystallization with different stoichiometric ratios of pyromellitic dianhydride, *J. Mol. Struct.* 1200 (2020) 127086.
- [17] M. Mukaida, Y. Watanabe, K. Sugano, K. Terada, Identification and physico-chemical characterization of caffeine–citric acid co-crystal polymorphs, *Eur. J. Pharmaceut. Sci.* 79 (2015) 61–66.
- [18] Q. Feng, M.L. Wang, B.L. Dong, J. He, C.X. Xu, Polymorphism and solvates of 1-acetyl-3-(phenyl)-5-(1-pyrenyl) pyrazoline: the structures, thermal and optical-physical properties, *CrystEngComm* 20 (2018) 661–667.
- [19] Q. Feng, M.L. Wang, B.L. Dong, J. He, C.X. Xu, Regulation of arrangements of pyrene fluorophores via solvates and cocrystals for fluorescence modulation, *Cryst. Growth Des.* 13 (2013) 4418–4427.
- [20] Q. Feng, M.L. Wang, B.L. Dong, C.X. Xu, J. Zhao, H.J. Zhang, Tuning solid-state fluorescence of pyrene derivatives via a cocrystal strategy, *CrystEngComm* 15 (2013) 3623–3629.
- [21] T.V. Timofeeva, V. Sena, B.B. Averkiev, S.N. Bejagam, M. Usman, A.V. Krivoshein, Unusual polymorphs of rac-3-phenylpyrrolidine-2, 5-dione with Z' = 1, 2, and 3, *CrystEngComm* 21 (2019) 6819–6829.
- [22] Q. Feng, M.L. Wang, C.X. Xu, A. Khan, X.J. Wu, J. Lu, X. Wei, Investigation of Molecular Arrangements and Solid-State Fluorescence Properties of Solvates and Cocrystals of 1-Acetyl-3-Phenyl-5-(9-anthryl)-2-pyrazoline, *CrystEngComm* 16 (2014) 5820–5826.
- [23] G.M. Sheldrick, Crystal structure refinement with SHELXL, *Acta Crystallogr.* 71 (2015) 3–8.
- [24] A.L. Spek, Platon SQUEEZE: a tool for the calculation of the disordered solvent contribution to the calculated structure factors, *Acta Crystallogr.* 71 (2015) 9–18.
- [25] D. Aulakh, A.P. Nicoletta, J.B. Pyser, J.R. Varghese, M. Wriedt, Design, structural diversity and properties of novel zwitterionic metal–organic frameworks, *Dalton Trans.* 46 (2017) 6853–6869.
- [26] R. Rajan, T.R. Ravindran, V. Venkatesan, V. Srihari, K.K. Pandey, S. Chandra, K.K. Mishra, A.A. Vargeese, New high pressure phases of energetic material TEX: evidence from Raman spectroscopy, X-ray diffraction, and first-principles calculations, *J. Phys. Chem.* 122 (2018) 6236–6242.
- [27] S.W. Ng, SQUEEZE for treating severely disordered solvent molecules in the refinement of the otherwise ordered crystal structures of [Cd(C<sub>12</sub>H<sub>10</sub>N<sub>4</sub>)(C<sub>15</sub>H<sub>9</sub>O<sub>2</sub>)<sub>2</sub>(CH<sub>3</sub>OH)]<sub>0.5</sub>H<sub>2</sub>O and [Cd(C<sub>12</sub>H<sub>10</sub>N<sub>4</sub>)<sub>1.5</sub>(C<sub>15</sub>H<sub>9</sub>O<sub>2</sub>)<sub>2</sub>] CH<sub>3</sub>OH, *Macedonian J. Chem. Eng.* 34 (2015) 57–61.
- [28] H. Abourahma, D.S. Cocuzza, J. Melendez, J.M. Urban, Pyrazinamide cocrystals and the search for polymorphs, *CrystEngComm* 13 (2011) 6442–6450.
- [29] B. Zhu, X.X. Fang, Q. Zhang, X.F. Mei, G.B. Ren, Study of crystal structures, properties, and form transformations among a polymorph, hydrates, and solvates of apatinib, *Cryst. Growth Des.* 19 (2019) 3060–3069.